JOURNAL OF MODERN OPTICS, 1990, VOL. 37, NO. 4, 555–573

Nonlinear properties of silica and air for picosecond ultraviolet pulses

I. N. ROSS, W. T. TONER, C. J. HOOKER, J. R. M. BARR† and I. COFFEY

Central Laser Facility, Rutherford Appleton Laboratory, Chilton, Didcot, Oxon OX11 0QX, England

Abstract. The nonlinear power limiting processes in silica and air are investigated for picosecond pulses at the KrF wavelength. The two-photon absorption coefficient and the nonlinear refractive index in silica are measured to be 0·06 cm GW^{-1} and $1{\cdot}7 \times 10^{-13}$ e.s.u. respectively. A mechanism for the rapid spectral broadening in air based on Raman-enhanced four-wave mixing is proposed. Experimental evidence supporting this hypothesis is presented.

1. Introduction

The current interest in excimer laser systems operating at terawatt power with picosecond or subpicosecond pulse durations has required increasing attention to the nonlinear processes occurring in materials through which the laser beam travels. Ultimately the power and energy achievable from such systems is limited by these nonlinear processes. The materials of interest for these lasers are fused silica, fluoride crystal optics, the laser medium, air and other gases such as helium and Raman media. Several nonlinear processes must be considered and the dominant mechanism identified. This may vary from material to material and wavelength to wavelength. We can identify the principal competing nonlinear effects for picosecond pulses as: self-focusing, Raman generation, spectral broadening, extreme spectral broadening or continuum generation, and nonlinear absorption. These processes have been considered both theoretically and experimentally but there is not sufficient experimental data in the ultraviolet, or sufficiently well understood theory, to enable a proper optimisation of high-power excimer laser systems, or to estimate the maximum achievable power from such a system.

This paper reports a number of measurements of the nonlinear properties of silica and air at ultraviolet wavelengths using short-pulse lasers. Some measurements have been reported by various groups [1–8, Y.P. Kim and M. H. R. Hutchinson, private communication] but the available information is not sufficiently complete for many purposes. To add to the available data we have measured both the nonlinear absorption coefficient and n_2 in silica at 249 nm. We have also measured the threshold for nonlinear effects in air at this wavelength and have gained some insight into the processes occurring at this threshold.

2. Theoretical considerations

(a) *Nonlinear absorption*

There are a number of possible mechanisms for nonlinear absorption, the most significant being two-photon absorption, three-photon absorption, single-photon absorption due to induced solarization following one- or two-photon absorption, and

† Department of Physics, The University, Southampton.

0950 0340/90 $3·00

excited state absorption followed two-photon absorption. It has been shown that it is possible to differentiate these processes [3] using particularly well controlled experimental techniques, but in silica at ultraviolet wavelengths it is sufficient to assume a two-photon absorption process in which the absorption coefficient varies linearly with intensity and the intensity transmission T_I is given by

$$T_I = \frac{I_l}{I_0} = \frac{1}{1 + I_0 \beta l}, \tag{1}$$

where I_0, I_l are the incident and transmitted intensities, β is the two-photon absorption coefficient and l is the path length in the nonlinear medium.

As the usual experimental parameter is energy, the relation between energy transmission T_E and two-photon absorption coefficient β must be found:

$$T_E = \frac{E_l}{E_0} = \frac{\int^A \int^t I_l \, dt \, dA}{\int\int I_0 \, dt \, dA} = \frac{\int\int [I_0/(1 + I_0 \beta l)] \, dt \, dA}{\int\int I_0 \, dt \, dA}. \tag{2}$$

T_E has been evaluated as a function of $I_0 \beta l$ for (1) the pulse square in space and Gaussian in time, (2) the pulse Gaussian in space and time, and the curves have been plotted in figure 1.

(*b*) *Self-focusing in the presence of nonlinear absorption*

The refractive index at high intensity is given by

$$n = n_0 + n_2 \langle E^2 \rangle = n_0 + \gamma I, \tag{3}$$

where $\gamma = 4{\cdot}2 \times 10^6 \, (n_2/n_0)$ for I in GW cm^{-2} and n_2 in e.s.u. The primary effect of n_2 is to introduce an intensity dependent phase on the transmitted beam given by

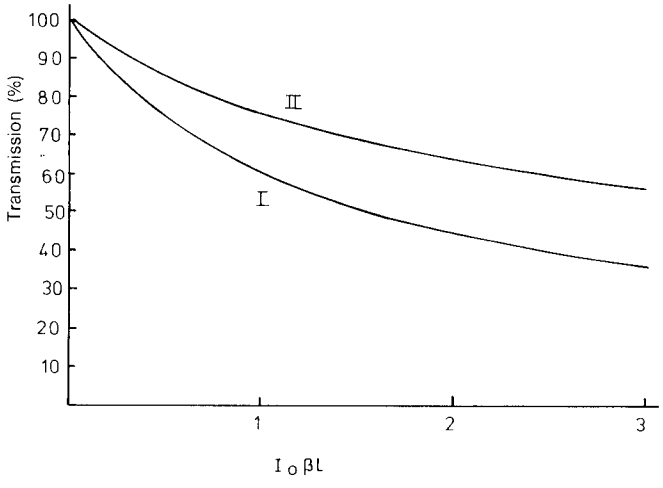

Figure 1. Transmission curves in the presence of two-photon absorption for two pulse shapes. I = Square space, Gaussian time: II = Gaussian space, Gaussian time.

$$\text{nonlinear phase} = \frac{2\pi}{\lambda_0} \int_l \gamma I \, \mathrm{d}l. \tag{4}$$

This integral is usually designated B and called the B integral. In the presence of nonlinear absorption only, we can substitute (1) into (4) to obtain

$$B = \frac{2\pi}{\lambda_0} \frac{\gamma}{\beta} \ln(1 + I_0 \beta l). \tag{5}$$

Thus, by time-resolved or time-integrated interferometry, the intensity dependent phase can be measured and a value of n_2 obtained.

Since the most serious effect of n_2 is generally beam filamentation, a relevant but indirect method of measuring n_2 is to observe the growth of intensity modulation on an intense beam. For a small modulation depth the growth G in modulation at a spatial frequency w has been shown [9] to be given by

$$G = \exp\left(\int 2\pi w \left[\frac{\gamma I}{n} - \left(\frac{\lambda w}{2} \right)^2 \right]^{1/2} \mathrm{d}l \right). \tag{6}$$

For

$$w = \frac{1}{\lambda} \left[\frac{2\gamma I}{n} \right]^{1/2}$$

there is maximum growth with

$$G_{\max} = \exp\left(\int k\mu \, \mathrm{d}l \right) = \exp B. \tag{7}$$

The presence of nonlinear absorption will inhibit self-focusing effects in two ways: filamentation will be inhibited through a damping term and the absorptive heating effect will lead to self-defocusing.

(i) *Damping effect of nonlinear absorption*

For the purposes of nonlinear beam propagation two-photon absorption can be represented as the imaginary part of a complex nonlinear refractive index. We replace n_2 by $n_2(1 + \mathrm{i}A)$ where $A = \beta / k_0 \gamma$. The simplest analysis of beam filamentation takes a strong beam travelling down the z axis and a weak beam travelling at an angle θ to this z axis. The magnitude of the field vector is then given by:

$$E = E_0 \exp[\mathrm{i}(kz - \omega t)] = C(1 + b) \exp[\mathrm{i}(kz - \omega t)], \tag{8}$$

where $C = \text{constant}$ and $b = a(z) \exp(\mathrm{i}k\theta x)$.

For such a beam the paraxial approximation to the wave-equation can be written:

$$V^2 E_0 + 2\mathrm{i}k \frac{\partial E_0}{\partial z} + k^2 \frac{n_2}{n_0} ([\mathrm{Re}\, E_0]^2 - C^2) E_0 = 0. \tag{9}$$

By substituting for E_0 from equation (8) into equation (9), we find the solution:

$$a(z) = a_0 \exp gz, \tag{10}$$

where

$$g = -(\beta I) \pm \left[(\beta I)^2 + 4\pi^2 w^2 \left(\frac{\gamma I}{n} - \left[\frac{\lambda w}{2} \right]^2 \right) \right]^{1/2}.$$

Figure 2 plots g for $\beta=0$ (no two-photon absorption) and for $\beta=k_0\gamma$. The effect on the growth of filaments is clearly substantial.

At a spatial frequency

$$\omega \simeq \frac{1}{\lambda}\left(\frac{2\gamma I}{n}\right)^{1/2}$$

the gain is maximum and is given by

$$g_{\max}=\{-\beta+[\beta^2+(k_0\gamma)^2]^{1/2}\}I. \tag{11}$$

Thus the maximum growth in modulation is given by

$$\frac{a(l)}{a_0}=\exp\left(\int g_{\max}\,\mathrm{d}l\right)=\exp(fB), \tag{12}$$

where

$$B=B\text{ integral}=\int k_0\gamma I\,\mathrm{d}l=\frac{k_0\gamma}{\beta}\ln(1+I_0\beta l),$$

$$f=-(\beta/k_0\gamma)+[(\beta/k_0\gamma)^2+1]^{1/2}.$$

(ii) *Thermal self-focusing*

Thermal heating due to the nonlinear absorption will result in a local reduction in refractive index (δn_{H}) and hence to a self-defocusing of the beam. By comparing the index changes due to this effect (δn_{H}) and due to n_2 (δn_I) we can estimate the magnitude of this damping effect

$$\frac{\delta n_{\mathrm{H}}}{\delta n_I}=\frac{\mathrm{d}n}{\mathrm{d}T}\,\frac{\mathrm{d}F/\mathrm{d}l}{\rho s\gamma I} \tag{13}$$

where $\mathrm{d}n/\mathrm{d}T$ is the temperature coefficient of the refractive index, ρ is the density, s is the specific heat, and $\mathrm{d}F/\mathrm{d}l$ is the absorbed fluence per unit depth in the material.

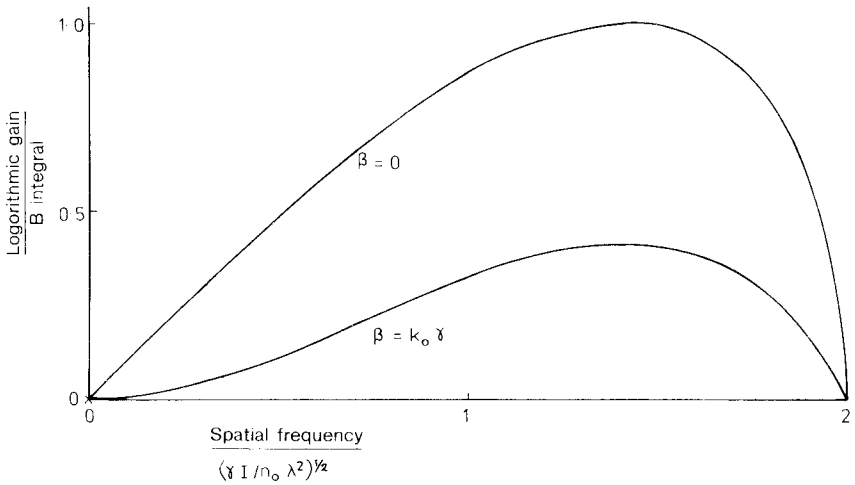

Figure 2. Effect on the filamentary gain of two-photon absorption.

For two-photon absorption

$$\frac{\mathrm{d}F}{\mathrm{d}l}=\frac{\mathrm{d}}{\mathrm{d}l}\left[\int_{\infty}^{t}\left(1-\frac{1}{1+\beta Il}\right)\mathrm{d}t\right]=\int_{\infty}^{t}\frac{I^2\beta\,\mathrm{d}t}{(1+I\beta l)^2}.$$

By using the maximum value of $\mathrm{d}F/\mathrm{d}l$, which occurs at $l=0$ and for $t\to\infty$ we obtain

$$\frac{\delta n_{\mathrm{H}}}{\delta n_I}=\frac{\mathrm{d}n}{\mathrm{d}T}\frac{\beta F}{\sqrt{2\gamma\rho s}} \tag{14}$$

for a Gaussian pulse.

By inserting the values for silica we obtain

$$\frac{\delta n_{\mathrm{H}}}{\delta n_I}=0{\cdot}7F$$

and in our experiments this effect is small since the intensities are about $10^{10}\ \mathrm{W\,cm^{-2}}$ for a 4 ps pulse duration, which gives $\delta n_{\mathrm{H}}/\delta n_I=0{\cdot}028$.

3. Measurement of nonlinear absorption at 249 nm

Figure 3 shows the arrangement used to measure the nonlinear absorption at 249 nm. A uniform circular beam of a few millijoules in 4 ps was used, the target intensity being varied by axial movement of the sample in a long focus telescope. The incident beam energy was monitored using an integrating photodiode and the transmitted beam energy was measured using a calibrated calorimeter. The amplified spontaneous emission energy was measured to be 5–10% of the short pulse energy and a correction applied. Measurements of transmitted energy with and without the test plate gave a number of values for the plate transmission as a function of the incident energy. These transmission values when corrected for the Fresnel reflection loss were applied to the curve of figure 1 to obtain values of $I_0\beta l$ and hence β. Figure 4 plots these values of β as a function of the intensity. The averaged value of β for fused silica was $0{\cdot}06\ \mathrm{cm\,GW^{-1}}$. We also note from figure 4 the apparent

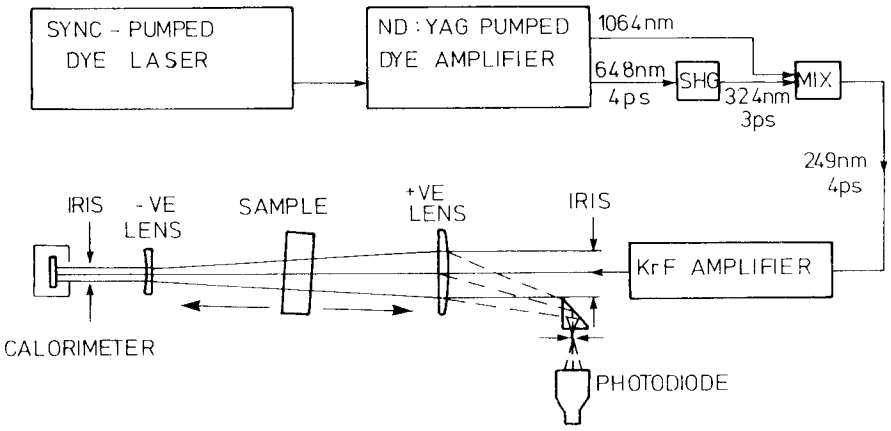

Figure 3. Schematic layout of measurement of nonlinear absorption at 249 nm.

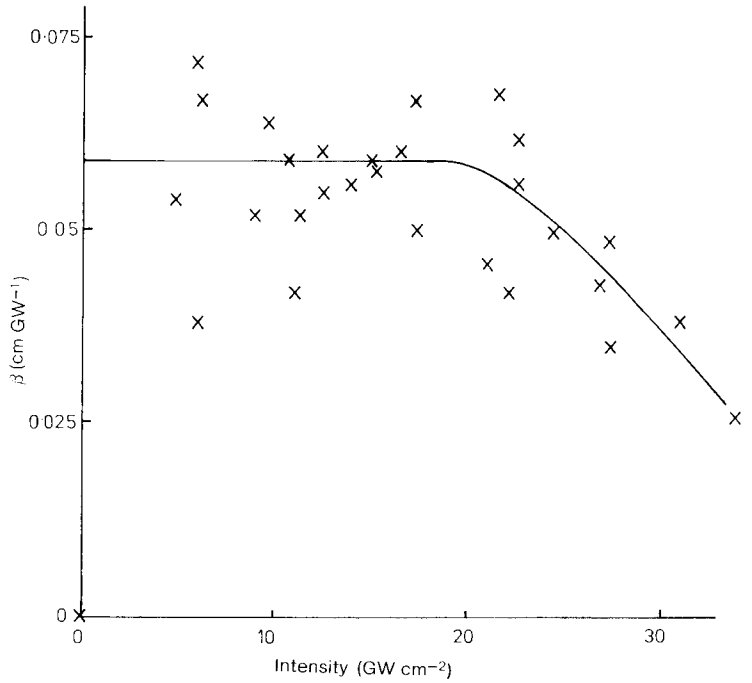

Figure 4. Measured values of the two-photon absorption coefficient as a function of intensity.

saturation of the absorption process at high intensity. The saturation of a nonlinear process has also been observed and commented on by Corkum [4], but this may also be caused by increasing competition with other loss processes.

The pulse duration was measured before the final amplification stage by a cross-correlation technique [10] in which the 249 nm pulse was mixed with the 324 nm pulse in a potassium dihydrogen orthophosphate (KDP) crystal to give a cross-correlation signal at 1064 nm. Assuming a Gaussian temporal profile, a mean pulse duration of 4 ps was calculated and this value was used in calculating intensities from measured values of fluence.

Errors in the measurements are almost entirely a result of the non-transform-limited nature of the pulses available from our laser source. The time–bandwidth product was about three times the transform-limited value for a Gaussian pulse. This resulted in increased uncertainty in determining the pulse duration from the average cross-correlation curve, since the half-intensity width is relevant for a transform-limited pulse while the quarter-intensity is appropriate for a noise burst. Using an intermediate width we estimate a $\pm 25\%$ uncertainty in the pulse duration for a Gaussian pulse. The pulse-to-pulse variation in duration and shape caused the large scatter in points in figure 4. The r.m.s. error in determining the mean from this scatter was $\pm 20\%$. Some error is also incurred by taking this mean value (not quite correct for a nonlinear process) and by assuming a Gaussian time profile in determing the pulse duration from the correlation curve and in calculating the curves of figure 1. Other errors are small. The error in our value for β is estimated to be $\pm 35\%$.

4. Measurement of nonlinear refractive index of silica at 249 nm

Two spatial techniques have been employed to make measurements of the nonlinear refractive index (n_2) of silica at 249 nm. A direct technique measuring the intensity-dependent phase-change and an indirect technique measuring the amplification of spatial intensity ripples on the beam. Although indirect, the latter is very relevant in that it measures directly the most serious effect of n_2. Our methods follow previously developed techniques for visible and infrared wavelengths [3].

(*a*) Figure 5 shows a 'common path' interferometer designed to give good contrast fringes of controllable spacing for broadband radiation at 249 nm. Figure 6 (*a*) shows the fringe pattern recorded using the broadband amplified spontaneous emission output of the excimer amplifier. The interferometer is designed so that only one of the two counter-propagating beams is at a high intensity in silica. All other beams are reduced to the 4% level by Fresnel reflections. Figure 6 (*b*) shows the fringe pattern for a low intensity beam and figure 6 (*c*) the fringe pattern at high intensity. The fringes can be seen to change in phase according to the local intensity. Measured values of this time-averaged phase change were inserted into equation (5) to derive a value for n_2. A correction factor to convert the time averaged to peak phase change was applied, assuming a Gaussian time profile, and peak intensities were derived from the measured fluences and the measured pulse duration. A mean value of $2{\cdot}0 \times 10^{-13}$ e.s.u. was obtained for n_2. Uncertainties in the measurement of the

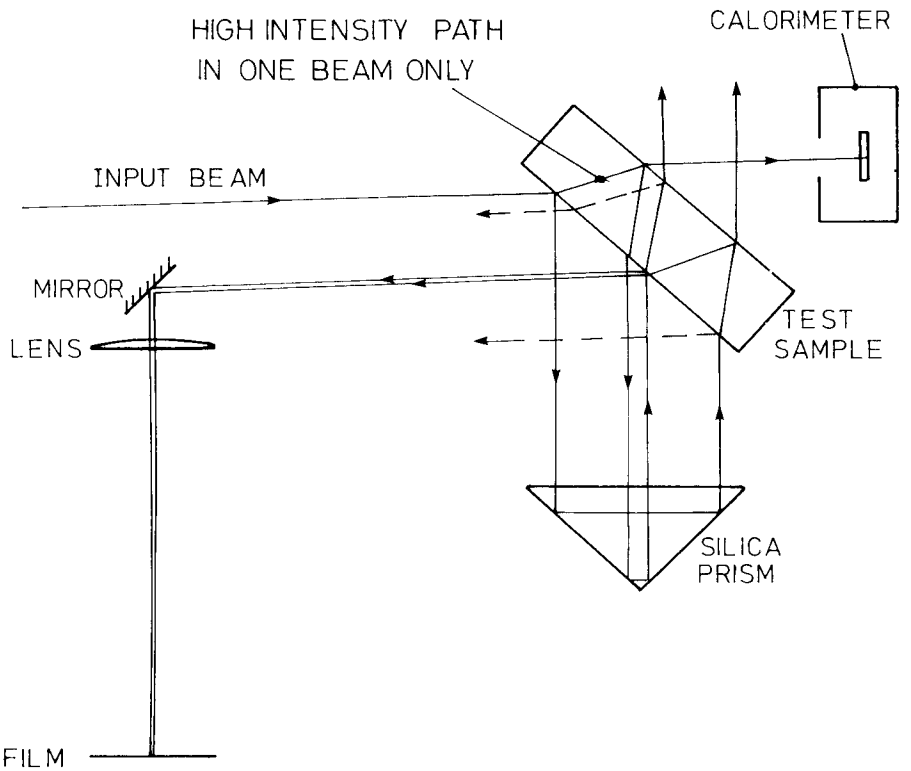

Figure 5. Schematic layout for common path interferometer for the measurement of nonlinear refractive index.

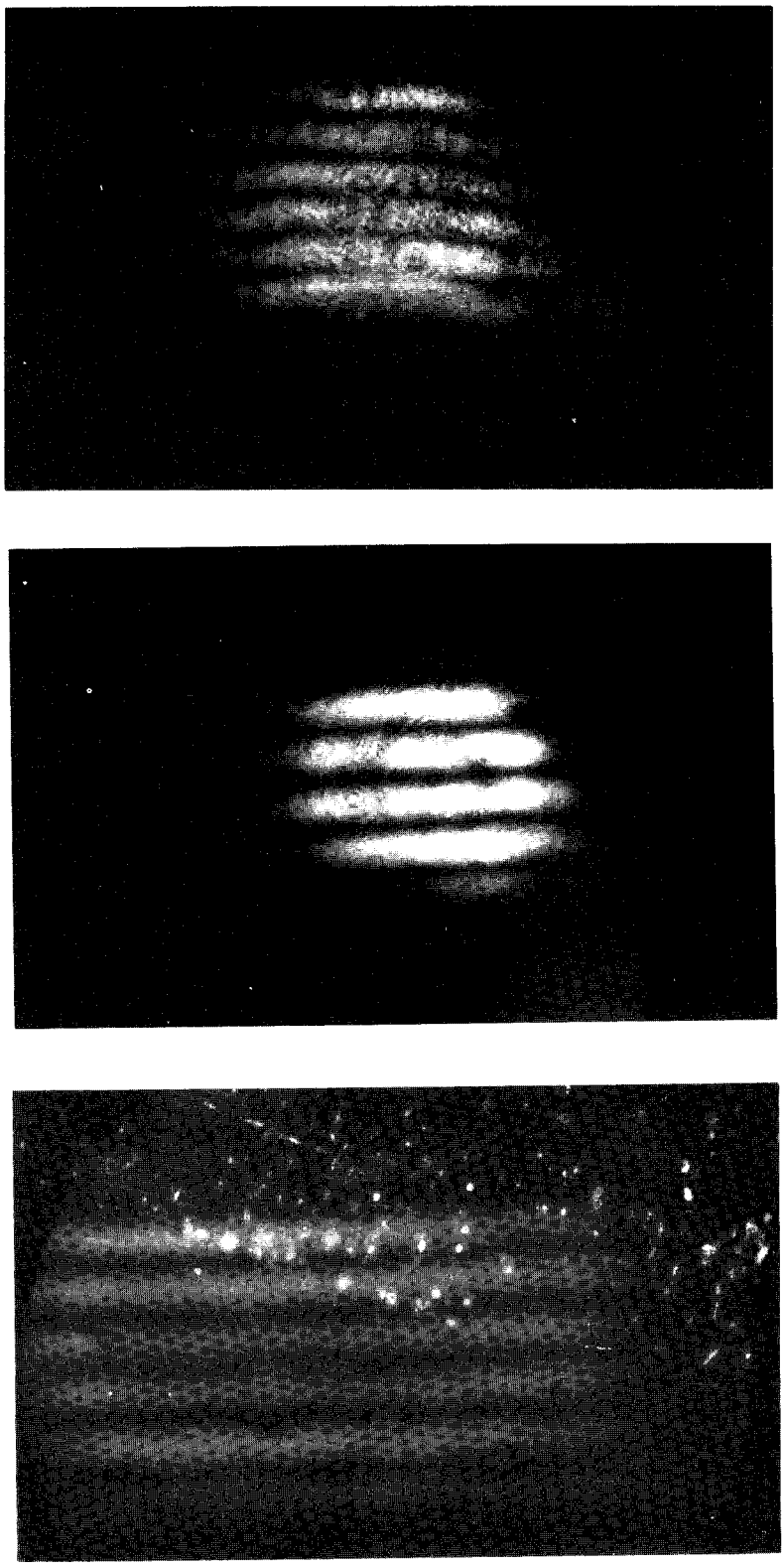

Figure 6. Interferograms recorded (*a*) using amplified spontaneous emission, (*b*) unamplified oscillator $\int I\,\mathrm{d}l = 0{\cdot}01\ \mathrm{GW\,cm^{-1}}$ using low-intensity beam, (*c*) amplified oscillator $\int I\mathrm{d}l = 10\ \mathrm{GW\,cm^{-1}}$ using high-intensity beam.

pulse duration, which were due to the assumption of a Gaussian time profile were similar to those of the nonlinear absorption measurement. There was a larger uncertainty resulting from the measurement of the small fringe shifts. Hence we estimate the error in the measurement of n_2 to be $\pm 40\%$.

(*b*) The second technique is illustrated in figure 7. Fringes of variable spacing and modulation depth were generated on the beam using Fresnel diffraction at a straight edge. Both front and back reflections from the test sample block were imaged onto film and simultaneously recorded. Figure 8 shows densitometer traces across images recorded in this way, demonstrating the enhancement of some spatial frequencies. Measurement of the spatial frequency showing maximum enhancement and measurement of the magnitude of this enhancement enabled two values of n_2 to be derived using equation (12) and the two values obtained were 1·0 and $1{\cdot}3 \times 10^{-13}$ e.s.u. respectively. The uncertainties in these values are similar to those of the previous section.

(*c*) A spectral technique may also be used to estimate n_2. The spectral width of a pulse is broadened as a result of the self-phase-modulation effect of n_2. The amount of broadening increases with increasing n_2 and can be calculated to obtain a quantitative value of n_2 from a measurement of the spectral broadening.

To enable an estimate of n_2 to be made, we assume an ideal (transform-limited) pulse with a Gaussian time envelope and a square spatial envelope given by

$$A(t) = A_0 \exp\left[-\tfrac{1}{2}(t/\tau)^2\right] \exp\left[\mathrm{i}(k_0 x - \upsilon_0 t - \phi)\right],$$

where τ is the intensity half-width at e^{-1} points; ϕ is the nonlinear phase change; υ_0 is the centre frequency; and A is the amplitude.

In the presence of self-phase-modulation (and in the absence of significant dispersion)

$$\phi = B \text{ integral} = B_0 \exp -(t/\tau)^2.$$

The spectral intensity can now be calculated using the Fourier transform to give

$$G(\upsilon) = gg^*,$$

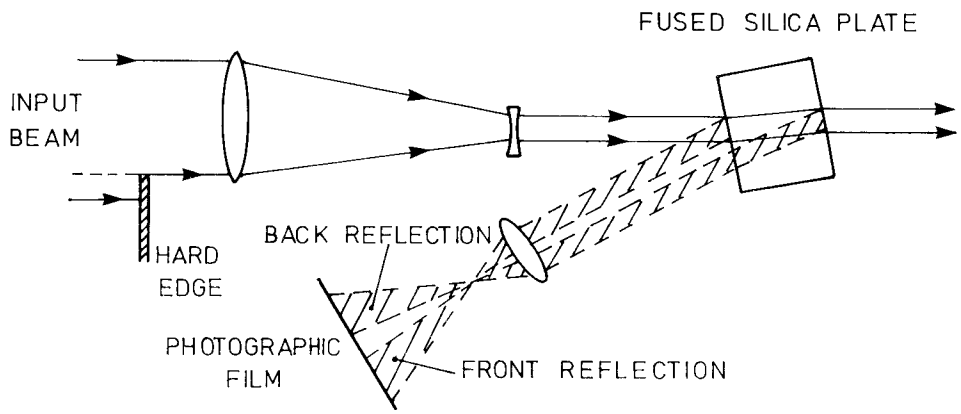

Figure 7. Arrangement for measuring filamentation.

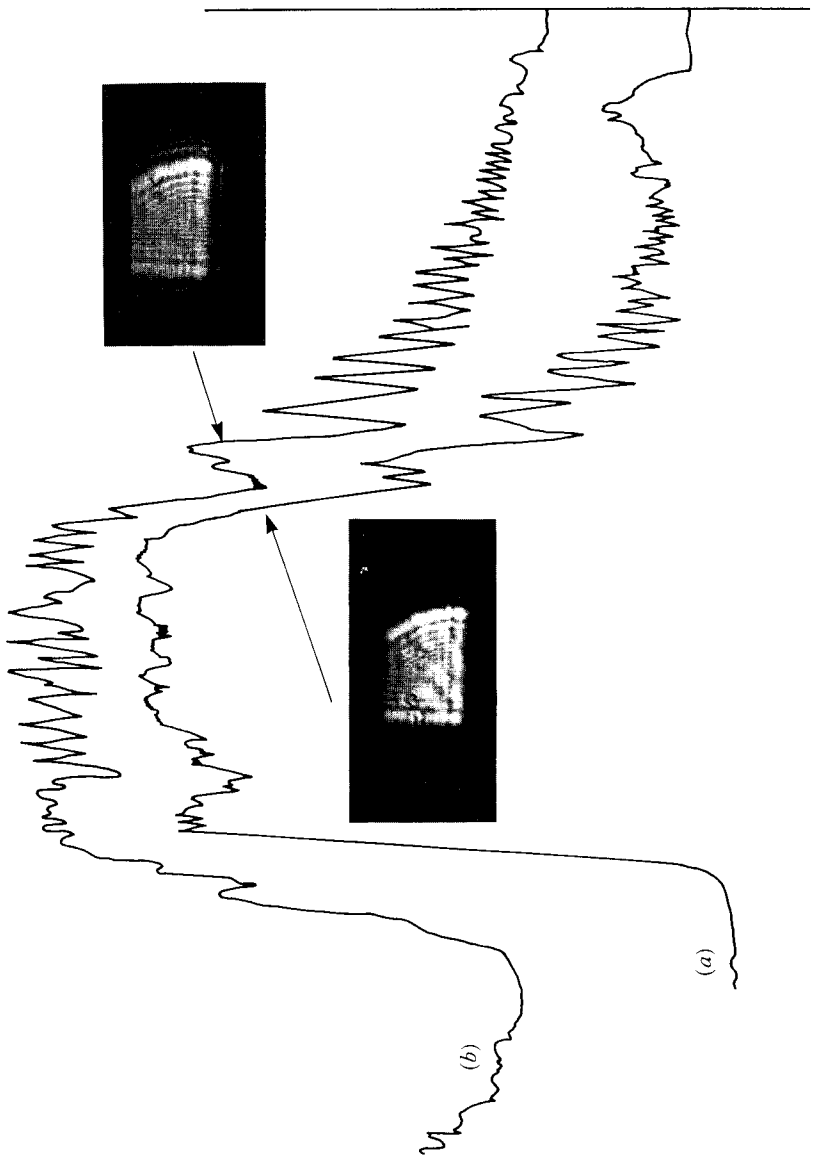

Figure 8. Measured intensity distributions before and after a sample showing filamentation. (*a*) front face reflection, (*b*) back face reflection.

where

$$g = g_0 \int_{-\infty}^{+\infty} \exp\left[-\tfrac{1}{2}(t/\tau)^2\right] \exp\left\{i[2\pi(\upsilon - \upsilon_0)t - B_0 \exp -(t/\tau)^2]\right\} dt.$$

$G(\upsilon)$ has been evaluated as a function of υ for different values of B_0 [13].

Figure 9 shows how the spectral width increases with the B integral and so provides the link for n_2 to be calculated from a measured spectral broadening. A useful analytical approximation to this curve for $0 < B < \sim 2$ is given by the formula

$$\frac{\text{Broadened linewidth}}{\text{Input linewidth}} = 1 + 0{\cdot}04B^2 + 0{\cdot}006B^6. \tag{15}$$

Figure 10 shows two spectra recorded from front and back reflections of a 20 mm thick sample of silica. The ratio of spectral widths gave a B-integral value of 1·8. Hence we obtained a value for $n_2 = 2{\cdot}8 \times 10^{-13}$ e.s.u. The uncertainty in this measurement is high and is not easily quantified for a non-transform-limited pulse as in our case. The fair agreement with our other measurements is consequently better than expected. This technique can, however, be recommended if transform-limited pulses are available.

5. Nonlinear refractive index for air at 249 nm

This refractive index for air at 249 nm may be estimated by observing the threshold power at which a spatially coherent focused beam will exhibit spectral broadening. This power should then be close to the 'critical power' for self-focusing (P_{CR}) which is approximated by

$$P_{CR} \approx \frac{\lambda^2}{n_2} \text{MW} \tag{16}$$

for λ in micrometres and n_2 in e.s.u. $\times 10^{13}$. Experimentally P_{CR} was measured by reducing an iris diaphragm in the focusing beam until spectral broadening was no longer observed and at this point the energy transmitted through the focus was

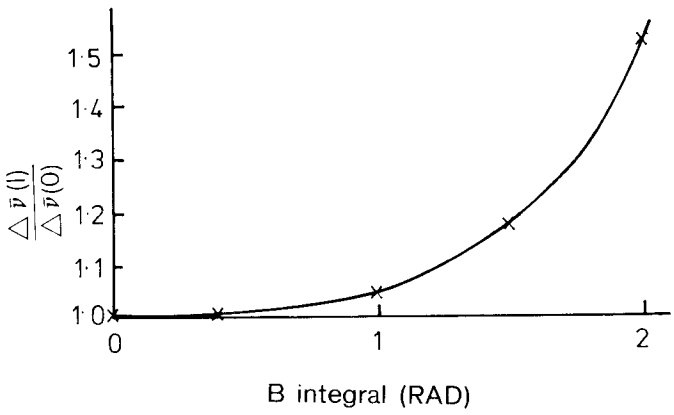

Figure 9. Calculated dependence of spectral broadening on B integral arising from self-phase-modulation.

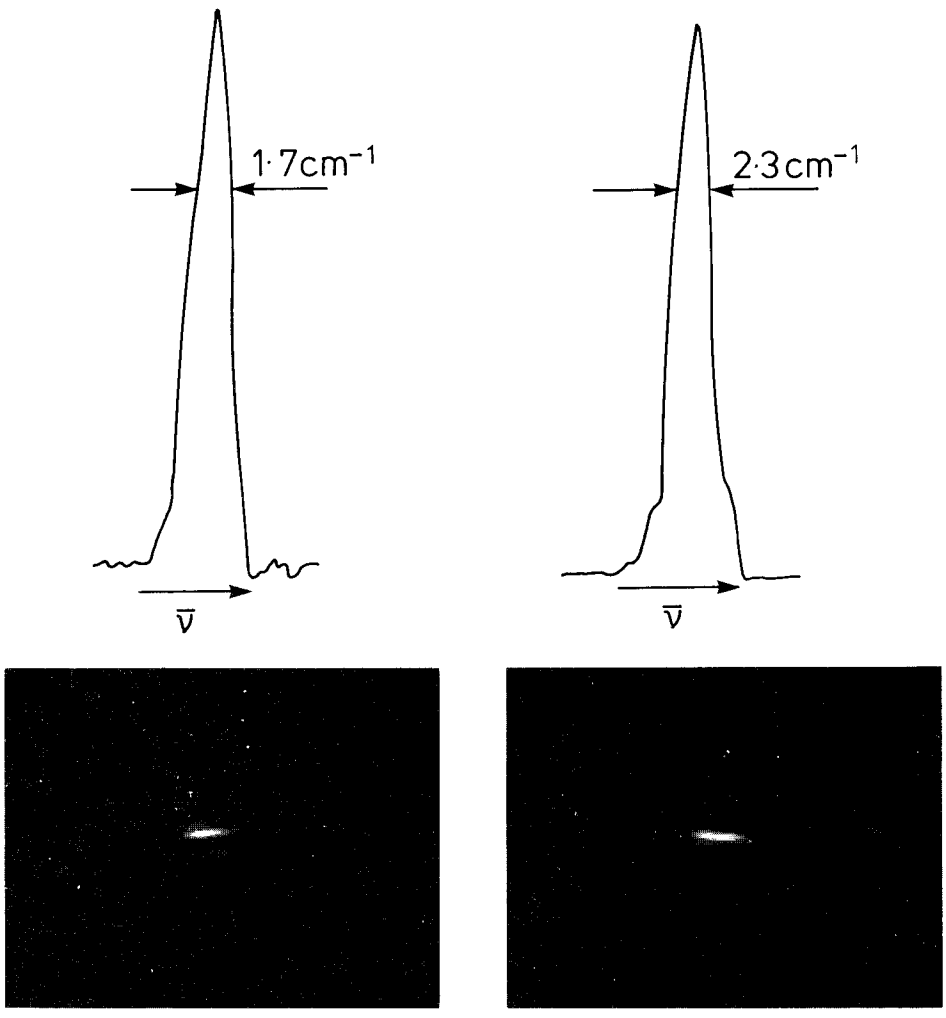

(*a*) Input spectrum (*b*) Output spectrum

Figure 10. Spectral broadening in silica at 249 nm due to self-phase modulation.

measured on a calorimeter. An energy threshold of 0·2 mJ was observed giving $P_{CR} = 50$ MW and hence (using equation (16)) a value for n_2 of $1{\cdot}2 \times 10^{-16}$ e.s.u.

Earlier measurements of n_2 for air [12] gave

$$n_2 = 2 \times 10^{-16} \text{ e.s.u. for } \lambda = 694 \text{ nm}.$$

Because the above estimate is based on an observable change, it will give an overestimate of the true threshold power. Hence it will give a lower limit for n_2. We will use the value of 2×10^{-16} e.s.u. for n_2 at 249 nm in subsequent calculations.

6. Broadband generation

Nonlinear spectral change can, under some conditions, be the dominant process and, even if it is not the dominant process, it may well affect beam propagation. The two principal spectral effects for short pulses are the generation of Stokes spectral

sidebands due to stimulated Raman scattering, and spectral broadening due to self-phase modulation, which is itself due to the nonlinear refractive index. The dominant process of the two is that which requires the lower value of $\int I\,dl$ at the 'threshold'.

The threshold for significant Raman generation is given by

$$\gamma_t \int I\,dl = 25, \tag{17}$$

where γ_t is the transient Raman gain coefficient $\approx \gamma_s/(1+5{\cdot}2T_2/t)$ see [13].

$$\therefore \int I\,dl = \left(25 + \frac{130T_2}{t}\right)\frac{1}{\gamma_s}, \tag{18}$$

where γ_s is the steady state gain coefficient; T_2 is the dephasing time $(1/\pi\Delta\upsilon_R)$; $\Delta\upsilon_R$ is the Raman linewidth; and t is the pulse length.

The self-focusing or self-phase modulation threshold taken to be at $B=1$ is given by

$$\int I\,dl = 60\lambda/n_2, \tag{19}$$

where λ is the wavelength in micrometres, and n_2 is the nonlinear index in e.s.u. $\times 10^{13}$.

Figure 11 plots the 'threshold' value of intensity length product obtained by inserting published values of material parameters for nitrogen into the above

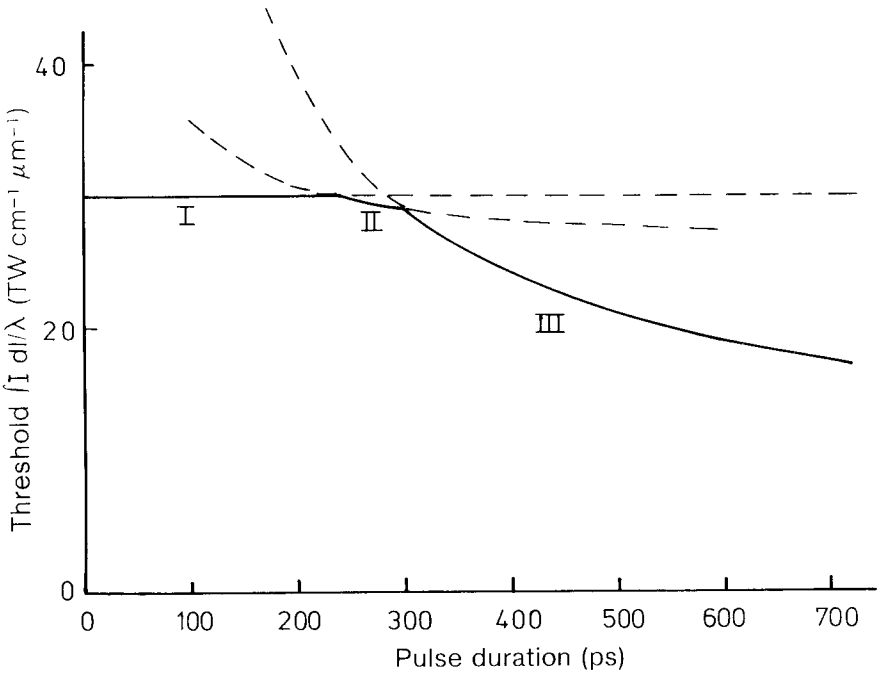

Figure 11. Dependence of threshold values of $\int I\,dl$ on pulse duration for self-focusing beam degradation and Raman losses. I, self-focusing: II, vibrational Raman; and III, rotational Raman.

equations. This shows, for nitrogen, how the dominant nonlinear process depends on the duration of the pulse.

(*a*) *Experiments at 249 nm in air*

A linearly polarised 4 ps pulse at 249 nm was focused in air using a 1 m focal length lens. A reflective grating working in third order dispersed the spectrum and gave a resolution of $<1\,\mathrm{cm}^{-1}$ for the full beam aperture. Figure 12 shows typical spectra at various beam intensities.

It can be seen from figure 11 that for these very short pulses vibrational Raman scattering should be stronger than rotational Raman scattering by virtue of its very short T_2 time (≈ 7 ps) and that self-focusing effects dominate. We would not expect to see the Raman–Stokes line in air with our short pulses and no evidence of its presence was found. The dominant effect in air, as shown by figure 12, is spectral broadening, which increased rapidly above a threshold value for $\int I\,\mathrm{d}l$ of $15\,\mathrm{TW\,cm}^{-1}$.

Since there is a possibility of four-wave-mixing processes contributing to the observed broadening, and since these have phase matching requirements that can make them dependent on the angular content of the beam, a second experiment was conducted in which the beam was not focused but propagated collimated over a long distance. Figure 13 shows the spectral broadening under these conditions. The threshold value for $\int I\,\mathrm{d}l$ was measured at $10\,\mathrm{TW\,cm}^{-1}$ and this lower value does suggest that effects with phase matching requirements must be considered as possible mechanisms for spectral broadening. Figure 13 also shows very much less broadening for longer pulses (40 ps). The reason for this may be due to the 40 ps pulses being of a much narrower spectral bandwidth ($0{\cdot}2\,\mathrm{cm}^{-1}$) and having time–bandwidth products which were much closer to the transform limit.

Figure 12 shows rapid broadening of the spectrum at increasing intensities. Figure 12 (*a*) shows a typical double line spectrum at low intensity. Figure 12 (*b*) shows that the spectral broadening is associated with sideband generation. Our interpretation of this process first suggested by Penzkofer *et al.* [14] is that there are efficient four-wave-mixing processes which enable pairs of wavelengths in the original spectrum to produce sidebands. This process should depend upon the third-order polarisabilities and be closely linked to similar processes such as self-focusing and self-phase-modulation. The observed thresholds are close to those expected for n_2 effects and some spectral broadening due to self-phase-modulation is generally seen as a precursor to 'continuum generation'.

The dominance of continuum generation over other processes including self-focusing depends upon a strong enhancement of the four-wave-mixing process and this can come from the close proximity of rotational Raman transitions. This 'off-resonant' Raman enhancement of four-wave-mixing has been considered by Dangor *et al.* [15] in a different context. They show that for the generation of a 10% side-band from a two-component spectrum

$$\frac{1}{2}\gamma_s \frac{\Gamma}{(\Gamma^2+\Delta\omega^2)^{1/2}} \int I\,\mathrm{d}l \approx (0{\cdot}1)^{1/2}, \tag{20}$$

where γ_s is the steady state Raman gain coefficient, Γ is the Raman half-linewidth, and $\Delta\omega$ is the off-resonant displacement.

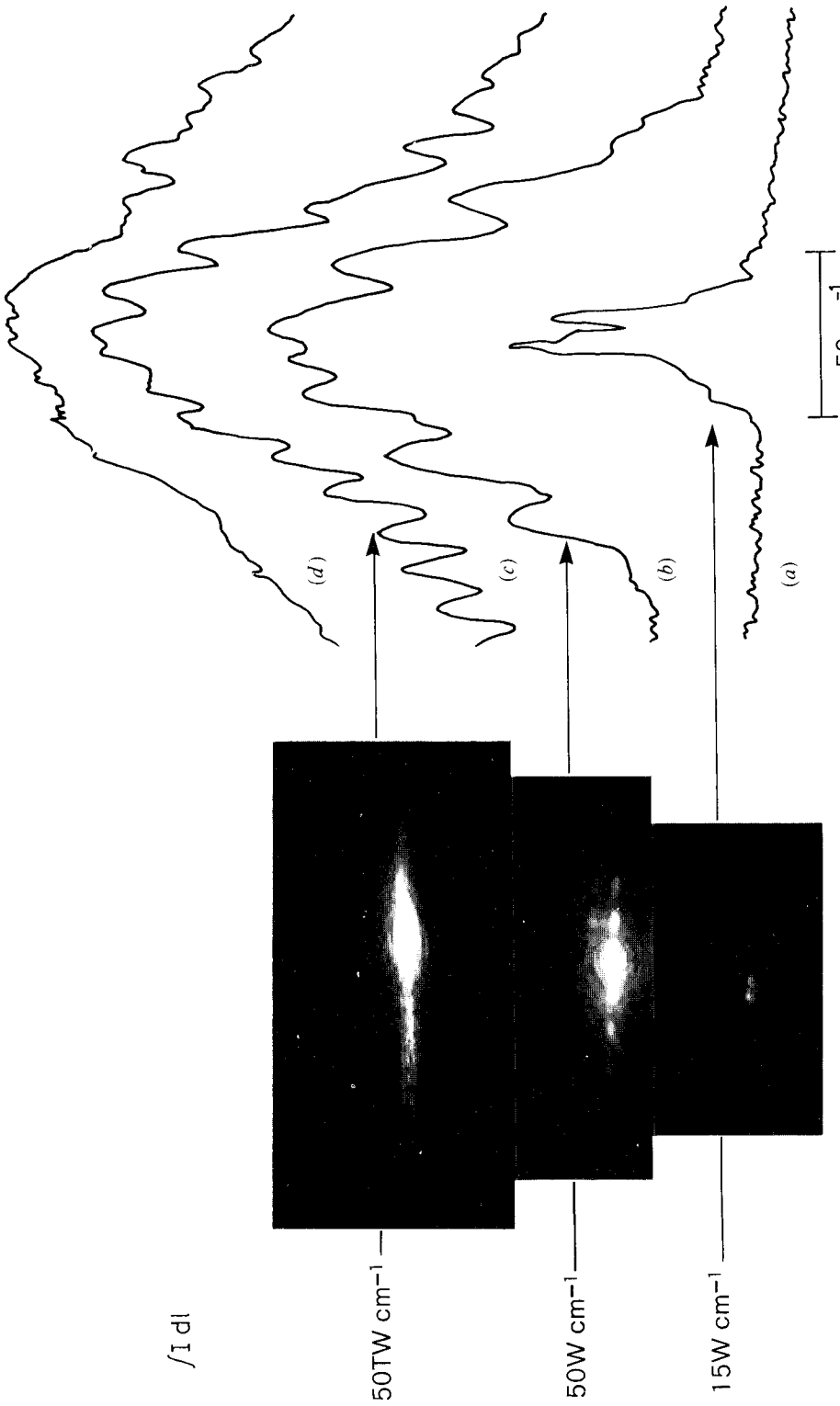

Figure 12. Spectral broadening in air at 249 nm at various intensities for focusing geometry. I = self-focusing, II = vibrational Raman, III = rotational Raman.

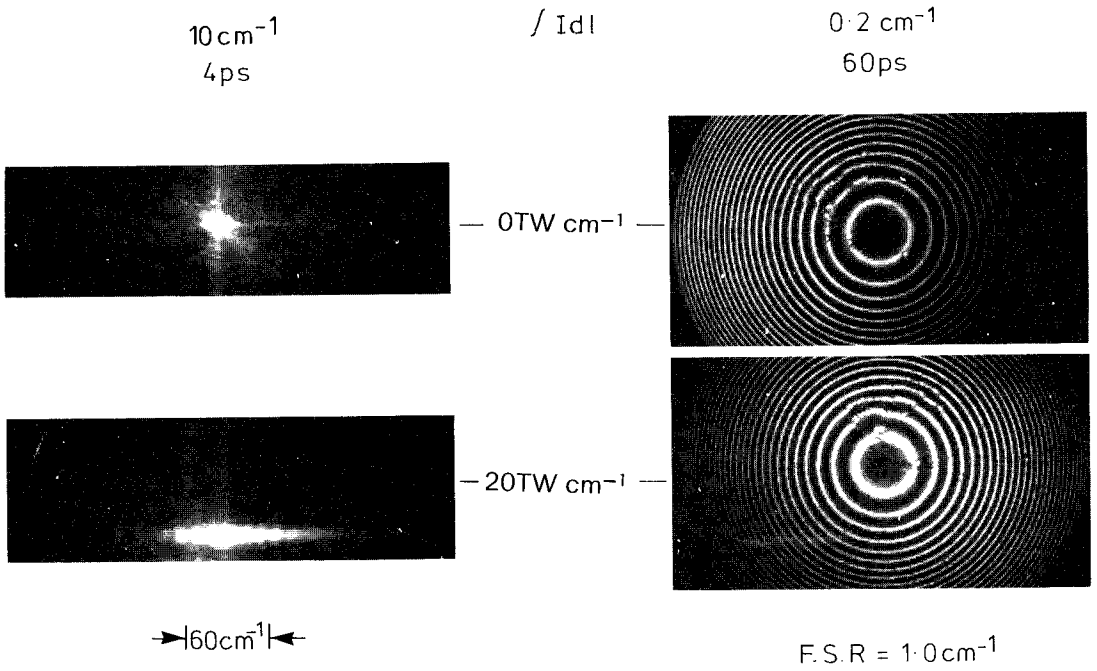

Figure 13. Spectral broadening in air at 249 nm at low and high intensity for collimated beams and for two pulse durations.

This is to be compared with the threshold for Raman generation of

$$\gamma_s \int I\,\mathrm{d}l \approx 25(1+5{\cdot}2T_2/t) \approx 130T_2.$$

The large difference in threshold is at once apparent under conditions for which the Stokes shift is not a large multiple of the pulse bandwidth.

Equation (20) applies to a single rotational transition. Inserting the values for the strongest rotational line in nitrogen (S [7]) together with our pulse parameters, the threshold condition, equation (20), reduces to $\int I\,\mathrm{d}l \approx 80\ \mathrm{TW\,cm^{-1}}$. Since there are a number of rotational Raman transitions with appreciable gain, it is necessary to sum the gain over all these lines. Thus our threshold condition now becomes

$$\int I\,\mathrm{d}l \sum_{\text{all lines}} \frac{\gamma_s \Gamma}{(\Gamma^2+\Delta\omega^2)^{1/2}} = 0{\cdot}63. \tag{21}$$

Making use of published data (see [16]), this summation has been evaluated over the rotational lines in nitrogen. The threshold conditions (equation (21)) reduce to

$$\int I\,\mathrm{d}l = 9\ \mathrm{TW\,cm^{-1}},$$

which compares well with the experimentally determined threshold value for $\int I\,\mathrm{d}l$ of $10\ \mathrm{TW\,cm^{-1}}$.

(*b*) *Polarisation dependence*

If the broadening mechanism is associated with stimulated rotational Raman scattering then there should be a strong polarisation dependence. In the case in

question we are concerned with the Raman gain for a beam with the same polarisation as the pump beam, then [17]

$$\frac{\gamma \text{ (circular)}}{\gamma \text{ (linear)}} = 0{\cdot}25. \tag{22}$$

Thus we would expect the threshold to increase by a factor of four to give a threshold value for $\int I \, dl$ of 60 TW cm^{-1}. Figure 14 shows spectral broadening for both linearly and circularly polarised beams. The suppression of this mechanism for circularly

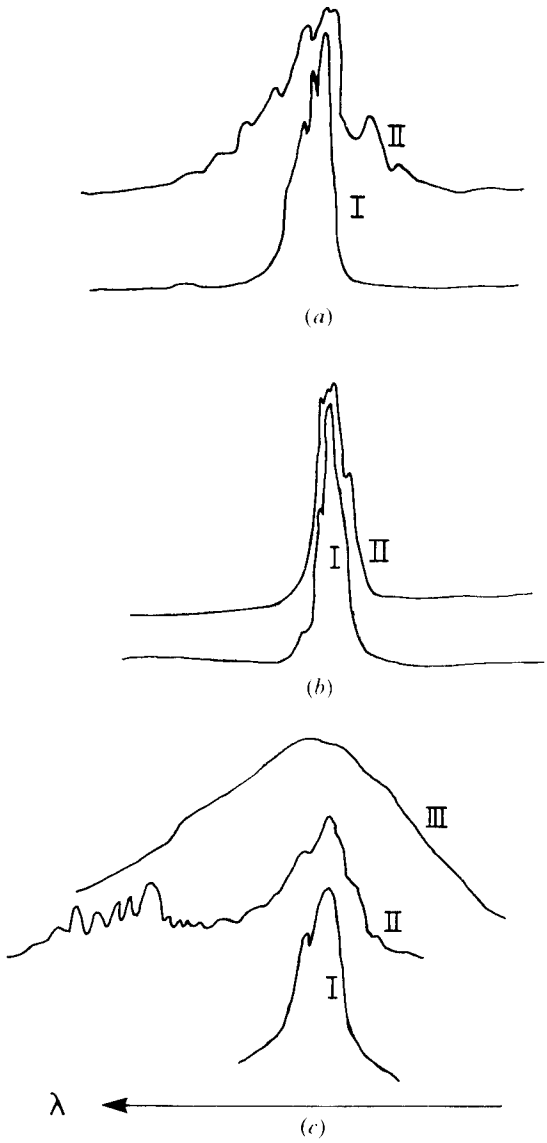

Figure 14. Spectral broadening in air at 249 nm for linear and circular polarisation of the beam. (*a*) Linear polarisation, $\int I \, dl = 145$ TW cm^{-1}, (*b*) circular polarisation, $\int I \, dl = 130$ TW cm^{-1}, (*c*) circular polarisation $\int I \, dl = 190$ TW cm^{-1}. I = Input spectrum, II = output spectrum, III = ASE spectrum.

polarised beams is immediately apparent and demonstrated a threshold ratio of about six, which was even higher than expected. The suppression is so strong that the threshold for generation of rotational Stokes lines can be reached (figure 14) before large spectral broadening severely depletes the beam.

7. Discussion of results

A number of measurements have been made of nonlinear optical effects which limit the peak power of ultraviolet lasers. These measurements have yielded values of the nonlinear absorption coefficient and the nonlinear refractive index and are included in the table. Limiting values of intensity length product are also given and it is these which determine the power limits of the laser.

At 249 nm, nonlinear absorption is the limiting effect in silica to the extent that effects resulting from n_2 can be disregarded. There was no detectable loss, within the intensity range available, to stimulated Raman scattering. This limit for silica is so restrictive that it is necessary to use crystal optics such as CaF_2 of MgF_2 wherever possible. These crystals can support intensities very much higher than that for silica. At 268 nm, which corresponds to the Raman–Stokes shifted line for a pump wavelength of 249 nm in methane, there is evidence [1] to suggest that silica can support very much higher values of $\int I\,\mathrm{d}l$. This is significant for laser systems utilising KrF-pumped Raman lasers. At this wavelength it is possible to work at significant values of B-integral. However, as discussed in section 2(*b*), the deleterious effects of a B-integral are less severe in the presence of nonlinear absorption. At 293 nm, severe spectral broadening has been observed as the limiting process, while at 308 nm, and from this wavelength to beyond 1 μm, it is self-focusing which sets the design limit on laser power.

The consensus of the measurements of n_2 in silica at 249 nm leads to a value of 1·5 $2{\cdot}0\times10^{-13}$ e.s.u. This is to be compared with measured values of about $1{\cdot}0\times10^{-13}$ e.s.u. from 308 nm to 1064 nm. Since n_2 can be regarded as a nonlinear four-wave-mixing process, with no change of frequency (i.e. $\omega+\omega-\omega\rightarrow\omega$), it is apparent that two-photon absorption ($\omega+\omega$) will exert a strong influence and that n_2 will significantly increase at wavelengths with significant two-photon absorption.

It has been shown that in air the dominant nonlinear process is dependent on pulse duration and that for short pulses the effects of n_2 dominate. No rotational or vibrational Raman spectra were observed, in agreement with this result. The threshold for spectral broadening was expected to be the same as that for self-focusing and this was observed. The value of n_2 obtained from this observation substantiated the value of 2×10^{-16} e.s.u. taken from the literature [14].

Summary of measurements on silica. TPA = two-photon absorption, SB = spectral broadening, SF = self-focusing.

Wavelength	249 nm	266/268 nm	293 nm	308 nm
TPA coefficient β (RAL) cm GW^{-1}	0·06	0·06	0·008	
β (other labs) cm GW^{-1}	0·045–0·06	0·02		0·007
$n_2\times10^{-13}$ e.s.u.	1·5–2·0			1·1
B integral at 20% loss from TPA	0·6	1·5	3·0	3·0
$\int I\,\mathrm{d}l$ limit in GW cm^{-1}	6	18	15	45
(limiting process)	(TPA)	(TPA)	(SB)	(SF)

The process of rapid spectral broadening occurring above the threshold is not explicable on the basis of self-phase-modulation. A possible explanation is proposed, which is based on the enhancement of four-wave-mixing effects due to the off-resonant gain from rotation Raman lines in nitrogen. This has been shown to match experimental observations of the threshold values of intensity length product ($\int I\,dl$) and of the polarisation dependence of this threshold intensity length product.

References

[1] Liu, P., Yen, L., and Bloembergen, N., 1975, *Appl. Optics*, **18,** 1015.
[2] Taylor, A. J., Gibson, R. B., and Roberts, J. P., 1988, *Optics Lett.*, **13,** 814.
[3] *Laser Program Annual Reports*, Lawrence Livermore National Laboratory, 1978/1982, UCRL-50021-78/82.
[4] Corkum, P., and Rolland, C., 1988, *Proc. SPIE*, **913,** 153.
[5] Taylor, R. S., Leopold, K. E., and Brimacombe, R. K., 1988, *Appl. Optics*, **27,** 567.
[6] Tomie, T., Okuda, I., and Yano, M., 1989, *Appl. Phys. Lett.*, **55,** 325.
[7] Simon, P., Gerhardt, H., and Szatmari, S., 1989, *Optics Lett.*, **14,** 1207.
[8] Ross, I. N., 1989, Annual Report to the Laser Facility Committee RAL-89-043.
[9] *Laser Program Annual Report*, Lawrence Livermore National Laboratory, 1973, UCRL-50021-73.
[10] Ross, I. N., Karadia, D., and Barr, J. M., 1989, *Appl. Optics*, **28,** 4054.
[11] Lehmberg, R. H., Reintjes, J., and Eckhardt, R. C., 1988, *Appl. Phys. Lett.*, **30,** 487.
[12] Vlasov, D. V., Garaev, R. A., Korobin, V. V., and Serov, R. S., 1979, *Soviet Phys. JETP*, **49,** 1033.
[13] Everall, N. J., Partanen, J. P., Barr, J. R. M., and Shaw, M. J., 1978, *Optics Commun.*, **64,** 393.
[14] Penzkofer, A., Laubereau, A., and Kaiser, W., 1973, *Phys. Rev. Lett.*, **31,** 863.
[15] Dangor, A. E., Dymoke-Bradshaw, A. K. L., Dyson, A., Garvey, T., Karttunen, S. J., Partanen, J. P., Salonaa, R. R. E., Cole, A. J., Danson, C., Edwards, C. B., and Evans, R. G., 1989, *J. Phys.* B, **22,** 797.
[16] Martin, W. E., and Winfield, R. J., 1988, *Appl. Optics*, **27,** 567.
[17] Rokni, M., and Flusberg, A., 1986, *IEEE J. quant. Electron.*, **22,** 1102.